



Alkyne-functionalized palladium nanoparticles: Synthesis, characterization, and electrocatalytic activity in ethylene glycol oxidation

Guoqiang He, Yang Song, Xiongwu Kang, Shaowei Chen*

Department of Chemistry and Biochemistry, University of California, 1156 High Street, Santa Cruz, CA 95064, USA

ARTICLE INFO

Article history:

Received 13 October 2012

Received in revised form 25 January 2013

Accepted 27 January 2013

Available online xxx

Keywords:

Palladium nanoparticle

Alkyne

Ethylene glycol

Electrooxidation

ABSTRACT

1-Octyne-stabilized palladium nanoparticles (PdHC8, core dia. 2.50 ± 0.28 nm) were prepared by a simple reduction procedure. FTIR studies showed that the self-assembly of 1-octyne onto the Pd nanoparticle surfaces involved the effective breaking of the terminal H—C \equiv bonds and the formation of Pd–vinylidene interfacial linkages by a tautomeric rearrangement process. With this conjugated metal–ligand interfacial bond, the nanoparticles exhibited unique photoluminescence properties that were analogous to those of diacetylene derivatives. Furthermore, thermogravimetric analysis showed that there were about 150 ligands per nanoparticle, with an average footprint of ca. 13 \AA^2 per capping ligand on the nanoparticle surface, consistent with a head-on configuration of the alkyne ligands on the Pd surface. Interestingly, the PdHC8 nanoparticles exhibited apparent electrocatalytic activity in the oxidation of ethylene glycol in alkaline media that was about twice that of commercial Pt/C, as manifested in cyclic voltammetric and chronoamperometric studies. Such an apparent improvement of the electrocatalytic activity was most probably ascribed to the partial removal of the alkyne capping ligands whereby the remaining molecules provided a relatively hydrophobic chemical environment and hence facilitated the removal of water generated from the oxidative dehydration reaction of ethylene glycol. Additionally, the enhanced electron density within the Pd metal cores as a result of the intraparticle charge delocalization between the particle-bound acetylene moieties might also facilitate the formation of Pd–C bonds in Pd-[C $_2$ H $_3$ (OH) $_2$] $_{\text{ads}}$, which was presumed to be the rate-determining step in ethylene glycol oxidation on Pd surfaces.

© 2013 Elsevier Ltd. All rights reserved.

1. Introduction

Alkaline membrane fuel cells (AFCs) have been hailed as a promising alternative to proton exchange membrane fuel cells (PEMFCs), primarily because of several apparent advantages. First, the reaction dynamics may be markedly facilitated in alkaline media, as compared to those in acidic media [1,2], and the enhanced electrode kinetics render it possible to use less platinum or even non-noble metals as effective electrocatalysts [3]. Second, the issues of fuel crossover may be minimized because the cell conductance is effected by the electro-osmosis of hydroxyl groups from the cathode to the anode. Third, by replacing the conventional liquid electrolytes with an alkaline anion exchange membrane, the precipitation of carbonates (CO $_3^{2-}$ /HCO $_3^-$) is minimized, leading to enhanced safety during fuel cell operation.

Toward this end, hydrogen has attracted great attention as an effective fuel candidate; yet the applications have been hindered by a range of critical issues involved in its production, purification, storage and distribution. Thus, a great deal of research has been

devoted to other liquid fuels, such as methanol, formic acid, ethanol, and ethylene glycol. Of these, the complete oxidation of methanol into CO $_2$ may be achieved by state-of-the-art PtRu alloyed catalysts [4,5]. Yet the wide-spread use of methanol is severely limited by its toxicity and potential detrimental impacts on the environment. In contrast, with its low toxicity and ready availability, ethanol has also been considered as a potential fuel for PEMFC applications [6,7]. For instance, a recent study has shown that with a PtSn catalyst, ethanol may be oxidized to acetic acid, acetaldehyde and CO $_2$ [8]. However, ethanol-based fuel cells in general exhibit only a low faradic efficiency as it is energetically difficult to break the C–C bond at low temperatures.

Within this context, the relatively good reactivity of ethylene glycol makes it an appealing candidate for fuel cells applications. It is less toxic than methanol; and with an alcohol group on both carbons, its specific energy is close to those of simple alcohols (5.2, 6.1, and 8.6 kWh/kg for ethylene glycol, methanol, and ethanol, respectively [9]). Notably, it has been proposed that ethylene glycol may be oxidized into oxalate species ($^-$ OOC–COO $^-$) [10], where 8 moles of electrons are produced with the consumption of one mole of ethylene glycol, suggesting a faradic efficiency of 80% (10 moles of electrons will be produced instead for the complete oxidation of one mole of ethylene glycol into CO $_2$) [11,12].

* Corresponding author. Tel.: +1 831 459 5841; fax: +1 831 459 2935.
E-mail address: shaowei@ucsc.edu (S. Chen).

In these fuel cell reactions, Pt-based catalysts typically exhibit a high intrinsic activity. However, they are vulnerable to surface poisoning by adsorbed CO (CO_{ad}), a reaction intermediate. In contrast, Pd is far less prone to CO_{ad} poisoning, in particular, in the short term [13,14]. Several other metals and alloys have also been examined for ethylene glycol electrooxidation, such as Au, Sn, Cd, Pb, PtRu and Pd [15–17]. For instance, Cherevko et al. [16] prepared Pd foams with a high surface area ($60 \text{ m}^2/\text{g}$) by hydrogen evolution-assisted electrodeposition, which displayed a high oxidation activity of C_2 alcohols (peak currents as high as 221 A/g for ethanol and 413 A/g for ethylene glycol). Wang [18] studied the effect of solution pH on the pathway of the electrooxidation of ethylene glycol on Pd by *in situ* FTIR spectroelectrochemistry, and showed that ethylene glycol electrooxidation on Pd proceeded in both strongly acidic and alkaline solutions. In strongly alkaline media, various intermediates were generated, but CO_2 was the ultimate product at high overpotentials. In contrast, in acidic solutions the main product was CO_2 with no detectable CO species. Note that in these earlier studies, the focus has primarily been placed on the impacts of the structures and elemental composition of the metal nanoparticles on the catalytic performance in ethylene glycol oxidation, and the effects of surface ligands (if any) remain largely unexplored. This is the primary motivation of the present study.

Recently, there emerges an effective approach where the nanoparticle electrocatalytic activities may be further manipulated and optimized by surface functionalization with selected organic ligands [19,20]. This is mainly ascribed to the deliberate manipulation of the nanoparticle core electronic structures which dictate the bonding interactions with the reactants, as well as to the third body effects that sterically impact the accessibility of surface catalytic sites, as evidenced in a series of recent studies [20,21]. Herein, we prepared stable palladium nanoparticles that were stabilized by the self-assembly of 1-octyne onto the Pd surface forming metal–vinylidene interfacial bonding linkages [22]. The resulting nanoparticles exhibited apparent electrocatalytic activity in ethylene glycol oxidation. Importantly, the observed activity was found to be markedly enhanced even compared to that of leading commercial Pt/C catalysts.

2. Experimental

2.1. Chemicals

Palladium chloride (PdCl_2 , 59% Pd, ACROS), hydrochloric acid (HCl, ACS Reagent, Sigma–Aldrich), sodium borohydride (NaBH_4 , 98%, ACROS), sodium hydroxide (NaOH, ACROS), 1-octyne (97%, Aldrich), and ethylene glycol (99+%, ACROS) were used as received. A commercial Pt/C catalyst was purchased from Alfa Aesar (20 wt.%, HiSPEC™3000, Johnson Matthey). Solvents were acquired at the highest purity available from commercial sources and used without further treatments. Water was supplied by a Barnstead Nanopure water system ($18.3 \text{ M}\Omega \text{ cm}$).

2.2. Synthesis of 1-octyne-functionalized palladium nanoparticles

In a typical reaction, a H_2PdCl_4 solution was first prepared by dissolving PdCl_2 (0.1 mmol) in hydrochloric acid (1 mL) at 50°C . When cooled down to room temperature, the solution was mixed with 1 mmol of 1-octyne in 10 mL of tetrahydrofuran (THF) under magnetic stirring. Then 0.3 mmol of NaBH_4 dissolved in 2 mL of ethanol was added to the solution, leading to the formation of a dark brown solution that signified the reduction of H_2PdCl_4 into Pd nanoparticles. The solution was extracted to toluene with a separatory funnel, washed with Nanopure water several times, and dried by rotary evaporation. The remaining solids were then rinsed with

a copious amount of methanol to remove impurities and excessive free ligands. The purified nanoparticles were denoted as PdHC8 and were readily dissolved in apolar solvents such as chloroform, dichloromethane, toluene, THF, etc.

2.3. Spectroscopy

The morphology and sizes of the Pd nanoparticles were characterized by transmission electron microscopic studies (TEM, Philips CM300 at 300 kV). More than 300 nanoparticles were measured to obtain a size histogram. ^1H NMR spectroscopic measurements were carried out by using concentrated solutions of the nanoparticles in CDCl_3 with a Varian Unity 500 MHz NMR spectrometer. The absence of any sharp features indicated that the nanoparticles were free of excessive unbound ligands (Fig. S1 in the Supporting Information). UV–vis spectroscopic studies were performed with an ATI Unicam UV4 spectrometer using a 1 cm quartz cuvette with a resolution of 2 nm. Photoluminescence characteristics were examined with a PTI fluorospectrometer. FTIR measurements were carried out with a Perkin–Elmer FTIR spectrometer (Spectrum One, spectral resolution 4 cm^{-1}), where the samples were prepared by casting the particle solutions onto a KBr disk. Thermogravimetric analysis (TGA) was carried out by using a Perkin–Elmer Pyris 1 instrument at a heating rate of $10^\circ\text{C}/\text{min}$ under a nitrogen atmosphere.

2.4. Electrochemistry

Electrochemical tests were carried out in a standard three-electrode cell connected to a CHI 710C electrochemical workstation, with a Pt foil counter electrode and an RHE reference electrode. The working electrode was a glassy carbon disk electrode with a diameter of 5 mm (from Bioanalytical Systems). To prepare catalyst solutions for electrochemical tests, $10 \text{ mg}_{\text{Pd}}$ of the PdHC8 electrocatalysts was dispersed in 10 mL of chloroform. A calculated amount was then dropcast onto the surface of the glassy carbon electrode with a Hamilton microliter syringe. The electrocatalyst loading was $50 \mu\text{g}/\text{cm}^2$. Finally, a drop of a 0.5 wt.% Nafion suspension was added onto the electrode surface to prevent damage to the electrocatalyst layer. The commercial catalyst Pt/C was loaded onto the electrode surface in a similar fashion, also at a metal loading of $50 \mu\text{g}/\text{cm}^2$.

3. Results and discussion

The nanoparticle structures were first characterized by high-resolution transmission electron microscopic (HRTEM) measurements. Fig. 1(A) depicts a representative TEM micrograph of the PdHC8 nanoparticles. It can be seen that the nanoparticles were well dispersed, indicative of the effective passivation of the nanoparticles by the 1-octyne ligands. In addition, the nanoparticles exhibited well-defined crystalline lattice fringes with a spacing of 0.231 nm, which is consistent with the *d*-spacing of the (1 1 1) planes of *fcc* Pd. The resulting nanoparticles also exhibited a rather narrow core size distribution, as manifested in the core size histogram in panel (B), with the majority of the nanoparticles within the range of 2.2–2.8 nm in diameter. In fact, statistical analysis based on more than 300 nanoparticles showed that the average nanoparticle core size was $2.50 \pm 0.28 \text{ nm}$, somewhat smaller than that of commercial Pt/C catalysts ($3.30 \pm 0.42 \text{ nm}$) [21].

The structures of the organic capping ligands were then characterized by FTIR measurements. Fig. 2 shows the FTIR spectrum (black curve) of the PdHC8 nanoparticles, along with that of 1-octyne monomers (red curve). There are at least three aspects that warrant attention. First, monomeric 1-octyne exhibits a rather intense vibrational band at 3314 cm^{-1} and a moderate one at 1255 cm^{-1} . These are assigned to the vibrational stretch and

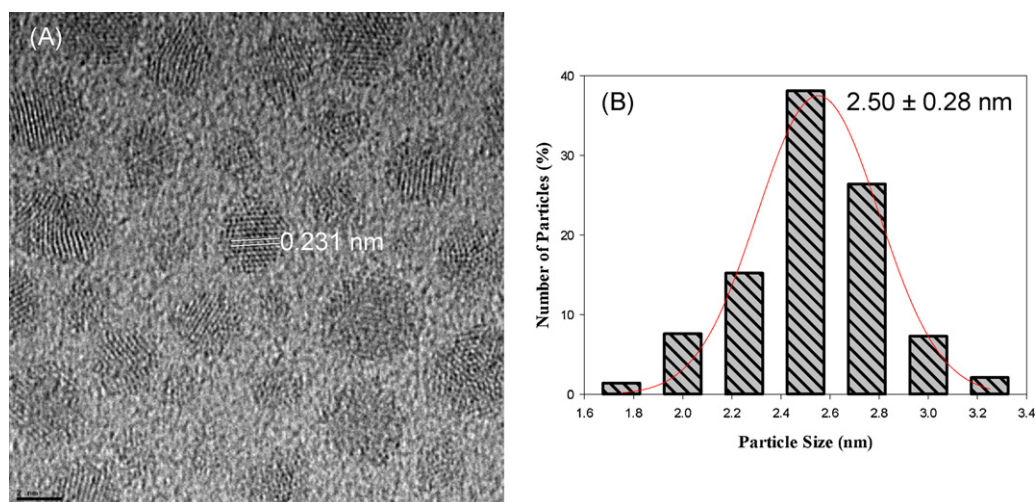


Fig. 1. (A) Representative TEM micrograph of PdHC8 nanoparticles and (B) the corresponding core size histogram. Scale bar in (A) is 2 nm; and red line in (B) reflects the Gaussian fit of the data. (For interpretation of the references to color in figure legend, the reader is referred to the web version of the article.)

the bend overtone of the terminal $\equiv\text{C}-\text{H}$ moieties, respectively. Yet these features vanished almost completely with the PdHC8 nanoparticles (the broad band between 3200 and 3600 cm^{-1} was due to residual water). This observation is most likely due to the self-assembly of 1-octyne molecules onto Pd surfaces where the $\equiv\text{C}-\text{H}$ bonds were effectively broken, along with the formation of a dynamic equilibrium between a palladium–vinylidene ($\text{Pd}=\text{C}=\text{CH}-$) linkage and a platinum–octynide ($\text{Pd}-\text{C}\equiv\text{C}-$) and palladium–hydride ($\text{Pd}-\text{H}$) bond at the metal–ligand interface by a tautomeric rearrangement process [22–24]. Second, one can see that the $\text{C}\equiv\text{C}$ vibrational stretch was well-defined at 2119 cm^{-1} for the 1-octyne monomers; whereas for the PdHC8 nanoparticles, it red-shifted to 2029 cm^{-1} . This suggests a diminishment of the bonding order of the terminal $\text{C}\equiv\text{C}$ moieties, most probably because of the effective intraparticle charge delocalization between the particle-bound ligands as a result of the conjugated metal–ligand interfacial bonds. Such a phenomenon has also been observed with Ru and Pt nanoparticles functionalized with similar 1-alkynes [22–24]. Third, the antisymmetric (d^-) and symmetric (d^+) vibrational stretches of the methylene (CH_2) moieties can be identified between 2800 and 3000 cm^{-1} for both the monomeric ligands and

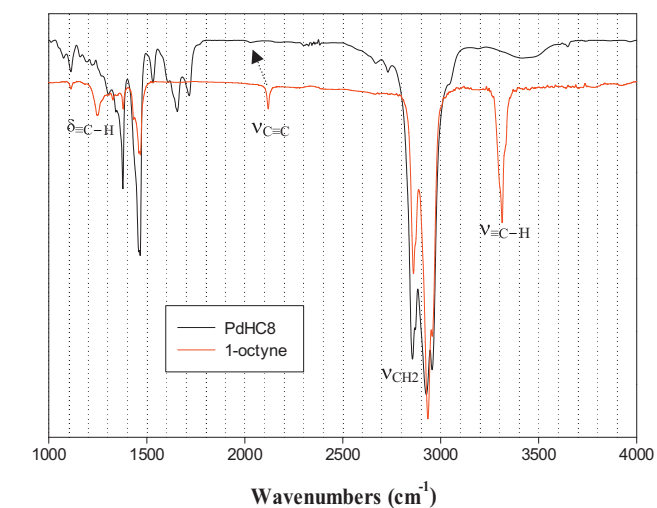


Fig. 2. FTIR spectra of PdHC8 nanoparticles (black curve) and 1-octyne monomers (red curve). (For interpretation of the references to color in figure legend, the reader is referred to the web version of the article.)

nanoparticles. However, a close examination shows a small red-shift for those of the nanoparticles (2926 cm^{-1} and 2855 cm^{-1}) as compared to those of the monomeric ligands (2935 cm^{-1} and 2861 cm^{-1}). This is consistent with the enhanced packing order of the ligands when they were bound onto the nanoparticle surface [23].

The number of capping ligands on the nanoparticle surface was then evaluated by TGA measurements. Fig. 3 shows the TGA curve of the PdHC8 nanoparticles at a heating rate $10^\circ\text{C}/\text{min}$. It can be seen that the sample weight started to decrease at around 140°C , exhibited an abrupt diminishment at 250°C , and remained practically unchanged at temperatures higher than 400°C . One may note that the transition temperature was somewhat higher than that observed with ruthenium nanoparticles functionalized by the same 1-octyne ligands (227°C), suggesting that the Pd–vinylidene bond might be somewhat stronger than the Ru–vinylidene counterpart [23]. Furthermore, from the weight loss (21.8%) of the PdHC8 nanoparticles, it can be estimated that there were about 150 ligands per nanoparticle, corresponding to an average footprint of ca. 13 \AA^2 per capping ligand on the nanoparticle surface, by taking into account the nanoparticle core diameter of 2.50 nm (Fig. 1). Note that this molecular footprint was slightly smaller than that observed for RuHC8 nanoparticles (15 \AA^2) [23]. The enhanced packing and hence van der Waals interactions between the neighboring

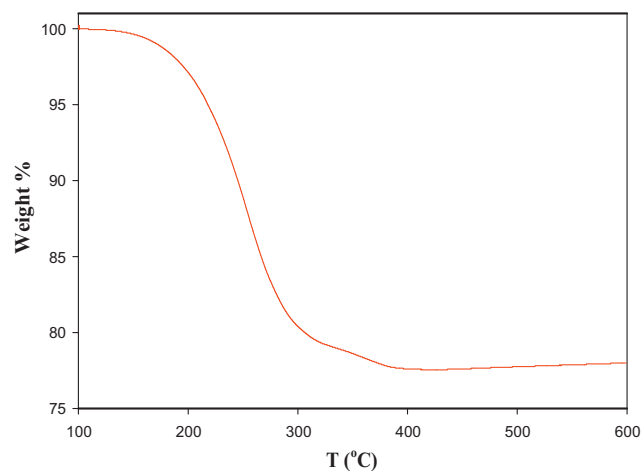


Fig. 3. TGA curve of PdHC8 nanoparticles at a heating rate $10^\circ\text{C}/\text{min}$.

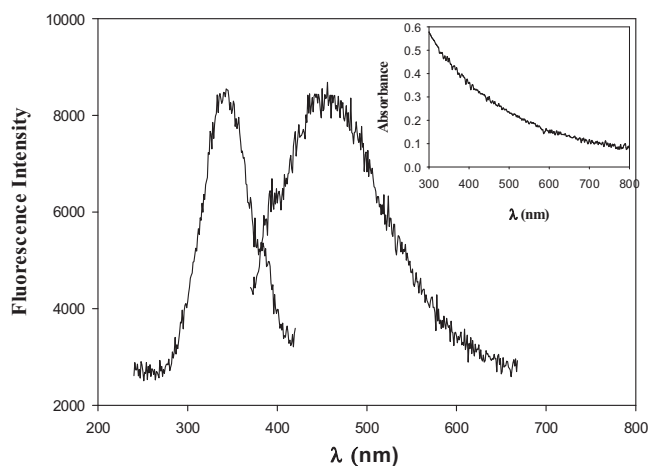


Fig. 4. Photoluminescence spectra of PdHC8 nanoparticles in chloroform at a concentration of 0.05 mg/mL. The corresponding UV-vis absorption spectrum was included as the figure inset.

particle-bound ligands might also contribute to the somewhat higher transition temperature as observed here.

With the conjugated metal–ligand interfacial bonding linkages, the PdHC8 nanoparticles exhibited unique optical properties. Fig. 4 shows the photoluminescence spectra of PdHC8 nanoparticles dissolved in CHCl_3 . A well-defined peak can be seen in both the excitation and emission spectra at 343 nm and 456 nm, respectively, whereas only an exponential decay profile was observed in UV-vis absorption measurements that might be accounted for by the Mie scattering theory of nanosized transition-metal particles (inset to Fig. 4). This is again attributed to the effective intraparticle charge delocalization between the particle-bound $\text{C}\equiv\text{C}$ moieties as a result of the palladium–vinylidene conjugated linkages, so that they behave analogously to diacetylene ($\text{C}\equiv\text{C}-\text{C}\equiv\text{C}$) derivatives. Consistent behaviors have also been observed with other transition-metal nanoparticles functionalized with similar terminal alkynes [22–24].

Interestingly, the PdHC8 nanoparticles prepared above exhibited apparent electrocatalytic activities in the oxidation of ethylene glycol. Fig. 5 shows the cyclic voltammograms of a glassy carbon electrode loaded with PdHC8 and commercial Pt/C electrocatalysts in 0.1 M NaOH solution at a potential sweep rate of 50 mV/s. Note that the currents have been normalized to the respective mass loading of the metal nanoparticle catalysts (ca. 9.8 μg of Pd or Pt). Unlike conventional surface-capping reagents (e.g., polymers) that bind strongly onto the nanoparticles and significantly diminish the accessibility of the nanoparticle surface, the surface of PdHC8 is fairly accessible for electrochemical reactions, and typically only about three potential cycles are needed to produce a stable voltammetric profile. In Fig. 5 (black curve), a well-defined cathodic peak at around +0.62 V can be observed which is assigned to the reduction of Pd oxide that was formed in the positive potential scan. Rand and Woods [25] have reported that a monolayer of Pd oxide would form on the Pd surface, and the reduction of this layer corresponds to a charge density of 424 $\mu\text{C}/\text{cm}^2$. This provides a convenient method to determine the effective electrochemical surface area (ECSA) of Pd, without the complication of surface contamination, as

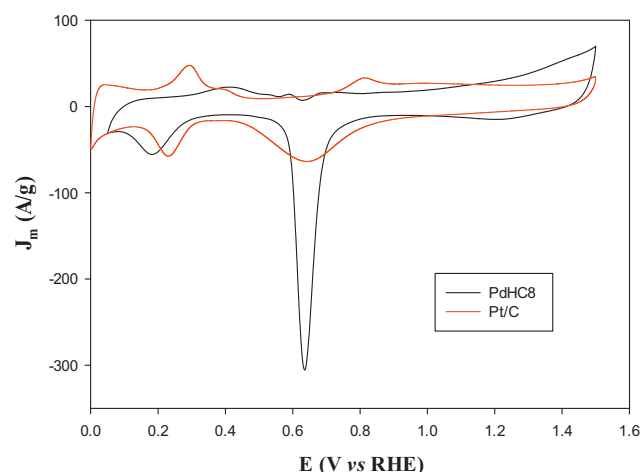


Fig. 5. Cyclic voltammograms of a glassy carbon electrode (dia. 5 mm) modified with PdHC8 and commercial Pt/C catalysts in an aqueous solution of 0.1 M NaOH. The metal loading was both ca. 9.8 μg . Potential sweep rate 50 mV/s.

observed in other methods (e.g., Cu UPD and CO stripping [26,27]). Thus, from Fig. 5, the specific ECSA of the PdHC8 nanoparticles-modified electrode was estimated to be 95.4 m^2/g , which is significantly higher than that (60 m^2/g) of Pd foams prepared by electrodeposition [16]. In addition, in comparison with the theoretical surface area of the PdHC8 nanoparticles (199.7 m^2/g) that was calculated on the basis of the particle average core diameter (2.50 nm, Fig. 1), this indicates that about 47.8% of the particle surface was accessible after the particles were loaded onto the electrode surface and underwent electrochemical treatments (Table 1). Note that in a previous study with platinum nanoparticles functionalized with acetylene derivatives, a significantly lower fraction of the metal nanoparticle surface was found to be electrochemically accessible [24].

In comparison, for the “bare” Pt/C-modified electrode (red curve), a pair of well-defined voltammetric peaks appeared at ca. +0.26 V, which are ascribed to the hydrogen adsorption/desorption on the platinum surface. On the anodic scan, the peak at +0.81 V is due to the formation of platinum oxide, and in the return sweep, the reduction of the platinum oxide is manifested as the peak at +0.64 V. Based on these voltammetric features the effective ECSA of the Pt/C modified electrode was evaluated to be 57.5 m^2/g , signifying that about 67.8% of the Pt nanoparticle surface was electrochemically accessible (Table 1), similar to that reported in a previous study [21].

The electrocatalytic activities of these two electrodes in the oxidation of ethylene glycol were then carried out and compared. Fig. 6 shows the corresponding voltammograms in an aqueous solution of 0.1 M ethylene glycol and 0.1 M NaOH at a potential sweep rate of 50 mV/s. It can be seen that at the PdHC8 nanoparticles-modified electrode (black curve), in the anodic scan, the oxidation of ethylene glycol started at around +0.459 V, and peaked at +0.851 V with a specific current density of 1084.0 A/g; and in the return scan, an oxidation current peak appeared at +0.720 V with a current density of 661.7 A/g. Remarkably, although still partially capped by the octyne ligands, the PdHC8 nanoparticles exhibited current densi-

Table 1

Summary of PdHC8 and Pt/C nanoparticles in the electrooxidation of ethylene glycol: electrochemical surface area (ECSA), fraction of the geometric surface area, onset potential (E_{onset}), anodic ($E_{\text{p,a}}$) and cathodic ($E_{\text{p,c}}$) peak potentials, anodic and cathodic peak currents normalized to ECSA ($J_{\text{s,a}}$ and $J_{\text{s,c}}$) and metal loading ($J_{\text{m,a}}$ and $J_{\text{m,c}}$).

	ECSA (m^2/g)	Fraction of geometric surface area	E_{onset} (V vs RHE)	$E_{\text{p,a}}$ (V vs RHE)	$J_{\text{s,a}}$ (A/m^2)	$J_{\text{m,a}}$ (A/g)	$E_{\text{p,c}}$ (V vs RHE)	$J_{\text{s,c}}$ (A/m^2)	$J_{\text{m,c}}$ (A/g)
PdHC8	95.4	47.8%	+0.459	+0.851	11.4	1084.0	+0.720	6.9	661.7
Pt/C	57.5	67.8%	+0.464	+0.922	9.4	542.8	+0.869	8.3	479.7

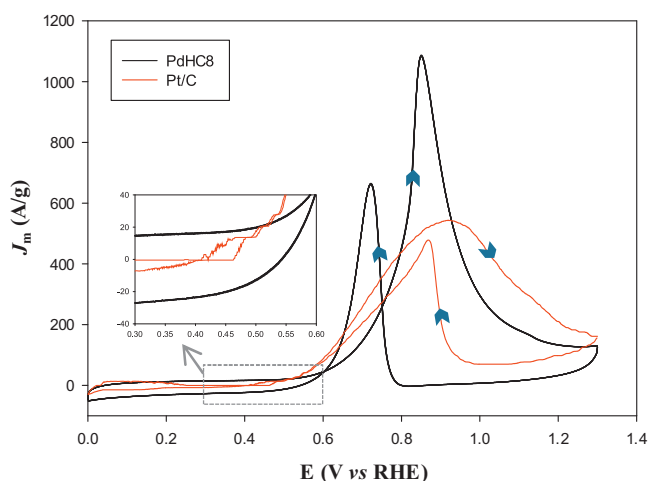


Fig. 6. Cyclic voltammograms of a glassy carbon electrode (dia. 5 mm) modified with PdHC8 and Pt/C catalysts in an aqueous solution containing 0.1 M ethylene glycol and 0.1 M NaOH. Potential sweep rate 50 mV/s. Other conditions were the same as those in Fig. 5. Inset shows the magnified region around the onset potentials.

ties that were significantly higher than that (413 A/g) observed by Cherevko et al. using Pd foams prepared by electrodeposition [16].

In addition, the catalytic performance of PdHC8 nanoparticles was also markedly enhanced as compared with commercial Pt/C catalysts, a leading catalyst for ethylene glycol electrooxidation. For the Pt/C-modified electrode (red curve), in the anodic scan, the oxidation of ethylene glycol started at ca. +0.464 V and the voltammetric current peaked at +0.922 V with a current density of 542.8 A/g. In the return scan, an oxidation peak also emerged at +0.869 V with a current density of 479.7 A/g. These results are summarized in Table 1. Note that these voltammetric features are consistent with those observed previously in the electrocatalytic oxidation of ethylene glycol at Pt or Pd electrodes [10,17,28]. Yet, whereas the onset potentials of ethylene glycol oxidation were rather consistent, the currents around the onset potentials rose much more rapidly with Pt/C than with PdHC8 (Fig. 6 inset), signifying a more rapid start of the electrooxidation of ethylene glycol; in contrast, at higher potentials (i.e., within the potential range of +0.6 to +0.8 V), in the anodic scan the currents of ethylene glycol oxidation exhibited a much steeper rise with PdHC8 than with Pt/C. These observations might be ascribed to more unified reaction pathways and products on PdHC8 than on Pt/C. Significantly, the peak potentials are apparently more negative with the PdHC8 nanoparticles than with Pt/C, in particular, in the cathodic scan; and the mass-normalized anodic peak current density ($J_{m,a}$) for PdHC8 is almost twice that for Pt/C, whereas the cathodic peak current density ($J_{m,c}$) is about 40% higher. These observations suggest that the PdHC8 nanoparticles exhibited a markedly better catalytic performance in the oxidation of ethylene glycol in alkaline media than leading commercial Pt/C catalysts (in Table 1, one may notice that the area-specific anodic and cathodic peak current densities ($J_{s,a} = 11.4 \text{ A/m}^2$ and $J_{s,c} = 6.9 \text{ A/m}^2$) of PdHC8 were both very comparable to those (9.4 A/m^2 and 8.3 A/m^2) of Pt/C, as depicted in Fig. S2, suggesting that the electrooxidation of ethylene glycol in alkaline media was almost equally facile on the PdHC8 and Pt/C nanoparticle surfaces; yet, for practical applications, mass-specific current density is typically used as the measuring yardstick to evaluate and compare the nanoparticle catalytic performance).

The stability of the electrocatalysts under continuous operating conditions was further examined by chronoamperometric measurements. Fig. 7 depicts the current–time curves of the two nanoparticle catalysts in the oxidation of ethylene

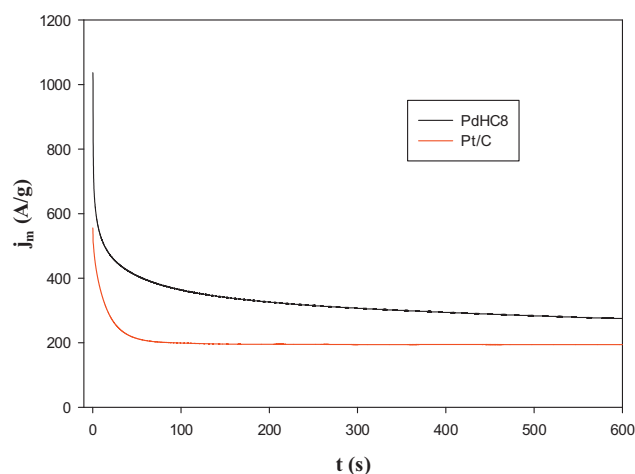


Fig. 7. Chronoamperometric profiles of a glassy carbon electrode (dia. 5 mm) modified with PdHC8 and Pt/C catalysts in an aqueous solution of 0.1 M ethylene glycol and 0.1 M NaOH by stepping the electrode potential from 0 to +0.80 V for 600 s. Other experimental conditions were the same as those in Fig. 6.

glycol by stepping the electrode potential from 0 to +0.8 V for 600 s. It can be seen that at both electrodes, the oxidation currents of ethylene glycol showed a rapid decrease within the first 100 s and then remained virtually invariant with time. Nonetheless, within the entire range of the test period, the PdHC8 nanoparticles (black curve) maintained a mass current density that was 1.5–2 times higher than that of commercial Pt/C (red curve), demonstrating significantly enhanced electrocatalytic activity and stability. For instance, at 600 s the oxidation current density at the PdHC8 nanoparticles-modified electrode was 275.3 A/g, whereas only 194.2 A/g at commercial Pt/C.

It should be noted that the reaction mechanism of ethylene glycol oxidation at noble metal electrode surfaces is rather complex and not yet fully understood [10,17,28]. Yet, prior research has shown that up to eight electrons might be involved in the oxidation of ethylene glycol with oxalate as the final product and glycol aldehyde, glycolate and glyoxalate as the intermediates and by-products [10]. In these reactions, the oxidative dehydration of adsorbed ethylene glycol has been proposed to be the rate-determining step, $\text{Pd}[\text{C}_2\text{H}_4(\text{OH})_2]_{\text{ads}} + \text{OH}^- \rightarrow \text{Pd}[\text{C}_2\text{H}_3(\text{OH})_2]_{\text{ads}} + \text{H}_2\text{O} + \text{e}^-$ [17]. Within this context, whereas the detailed reaction mechanism is not clear at this point, the enhanced catalytic activity of the PdHC8 nanoparticles, as compared with “naked” noble metal catalysts (e.g., Pd forms [16], or commercial Pt/C), may be attributed to the combined contributions from both the geometric as well as electronic effects. Specifically, with the partial removal of the organic capping ligands from the PdHC8 nanoparticle surface (Fig. 5), the remaining molecules offered a relatively hydrophobic environment on the Pd nanoparticle surface that facilitated the removal of H_2O generated in the dehydration reactions. Further contributions might arise from the intraparticle charge delocalization afforded by the $\text{Pd}=\text{C}=\text{CH}-$ conjugated interfacial linkages that facilitated the formation of $\text{Pd}-\text{C}$ bonds in $\text{Pd}[\text{C}_2\text{H}_3(\text{OH})_2]_{\text{ads}}$, as the $\text{Pd}-\text{C}$ bonds generally involve $d\pi$ electrons and the extended conjugation between the particle-bound acetylene moieties most likely increases the effective electron density within the Pd metal cores. While further research is desired to unravel the mechanistic insights, the results presented herein further demonstrate the unique advantages of deliberate organic functionalization of metal nanoparticle catalysts in the manipulation and enhancement of their electrocatalytic activities [20,21].

4. Conclusion

Palladium nanoparticles functionalized with 1-octyne (PdHC8) were prepared by a one-step reduction procedure. The nanoparticles exhibited an average core diameter of 2.50 ± 0.28 nm, as determined by TEM measurements. FTIR measurements showed that the 1-octyne molecules self-assembled onto the Pd surface most likely with the effective breaking of the $\equiv\text{C}-\text{H}$ bonds and the formation of a dynamic equilibrium between a Pd–vinylidene interfacial linkage and a palladium–octynide and palladium–hydride bond by virtue of a tautomeric rearrangement process. This was evidenced by the disappearance of the $\text{H}-\text{C}\equiv$ vibrational bands and an apparent red-shift of the $\text{C}\equiv\text{C}$ vibrational stretch from 2119 cm^{-1} to 2029 cm^{-1} , as compared to the vibrational features of the monomeric ligands. With these conjugated interfacial bonds, the nanoparticles exhibited interesting photoluminescence properties with a pair of well-defined excitation and emission peaks at 343 nm and 456 nm, respectively, that were analogous to those of diacetylene derivatives. Furthermore, TGA measurements showed that there were about 150 ligands per nanoparticle, corresponding to an average footprint of ca. 13 \AA^2 per capping ligand on the nanoparticle surface, consistent with a head-on configuration of the alkyne ligands on the Pd surface. Interestingly, the resulting nanoparticles exhibited apparent electrocatalytic activity in the oxidation of ethylene glycol in alkaline media. In comparison with commercial Pt/C catalysts, the PdHC8 nanoparticles displayed marked enhancement of the electrocatalytic performance, with an anodic peak that was ca. 70 mV more negative, and a mass-specific peak current density that was about twice as much. The PdHC8 nanoparticles were also found to exhibit enhanced stability in chronoamperometric measurements. Overall, the substantial improvement of the electrocatalytic activity of PdHC8 nanoparticles in the oxidation of ethylene glycol might be attributed to the partial removal of the organic capping ligands, whereby the remaining molecules provided a relatively hydrophobic environment for the effective removal of water generated in the oxidative dehydration of adsorbed ethylene glycol, as well as to the enhanced electron density of the Pd metal cores that facilitated the formation of Pd–C bonds in $\text{Pd}-[\text{C}_2\text{H}_3(\text{OH})_2]_{\text{ads}}$, which is presumed to be the rate-determining step in ethylene glycol oxidation on Pd surfaces. Taken together, these results suggested that deliberate functionalization of nanoparticle surfaces by selected functional ligands indeed might be exploited as a powerful and yet unconventional route toward the further improvement of the nanoparticle electrocatalytic performance in fuel cell electrochemistry.

Acknowledgments

This work was supported, in part, by the National Science Foundation (CHE-1012258, DMR-0804049, and CBET-1258839) and the ACS Petroleum Research Fund (49137-ND10). TEM studies were carried out at the National Center for Electron Microscopy, Lawrence Berkeley National Laboratory as part of a user project.

Appendix A. Supplementary data

Supplementary data associated with this article can be found, in the online version, at <http://dx.doi.org/10.1016/j.electacta.2013.01.134>.

References

- [1] Y. Wang, L. Li, L. Hu, L. Zhuang, J.T. Lu, B.Q. Xu, A feasibility analysis for alkaline membrane direct methanol fuel cell: thermodynamic disadvantages versus kinetic advantages, *Electrochemistry Communications* 5 (2003) 662.
- [2] C.-C. Yang, Preparation and characterization of electrochemical properties of air cathode electrode, *International Journal of Hydrogen Energy* 29 (2004) 135.
- [3] C. Bianchini, P.K. Shen, Palladium-based electrocatalysts for alcohol oxidation in half cells and in direct alcohol fuel cells, *Chemical Reviews* 109 (2009) 4183.
- [4] T. Frelink, W. Visscher, J.A.R. van Veen, Measurement of the Ru surface content of electrocodeposited PtRu electrodes with the electrochemical quartz crystal microbalance: implications for methanol and CO electrooxidation, *Langmuir* 12 (1996) 3702.
- [5] P. Waszczuk, A. Wieckowski, P. Zelenay, S. Gottesfeld, C. Coutanceau, J.M. Leger, C. Lamy, Adsorption of CO poison on fuel cell nanoparticle electrodes from methanol solutions: a radioactive labeling study, *Journal of Electroanalytical Chemistry* 511 (2001) 55.
- [6] R. Zheng, X. Zhou, S. Wang, T. Wen, C. Ding, A study of Ni + 8YSZ/8YSZ/La_{0.6}Sr_{0.4}CoO_{3-δ} ITSOFC fabricated by atmospheric plasma spraying, *Journal of Power Sources* 140 (2005) 217.
- [7] S.Q. Song, P. Tsiakaras, Recent progress in direct ethanol proton exchange membrane fuel cells (DE-PEMFCs), *Applied Catalysis B: Environmental* 63 (2006) 187.
- [8] S. Rousseau, C. Coutanceau, C. Lamy, J.M. Leger, Direct ethanol fuel cell (DEFC): electrical performances and reaction products distribution under operating conditions with different platinum-based anodes, *Journal of Power Sources* 158 (2006) 18.
- [9] C. Lamy, J.M. Leger, Fuel-cells – application to electric vehicles, *Journal de Physique IV* 4 (1994) 253.
- [10] W. Hauffe, J. Heitbaum, Electrooxidation of ethylene-glycol at platinum in potassium hydroxide, *Electrochimica Acta* 23 (1978) 299.
- [11] E. Santos, M.C. Giordano, Electrocatalytic oxidation of organic-molecules in alkaline-solutions. 2. Electroadsorption and electrooxidation of ethylene-glycol at platinum, *Electrochimica Acta* 30 (1985) 871.
- [12] R.B. de Lima, V. Paganin, T. Iwasita, W. Vielstich, On the electrocatalysis of ethylene glycol oxidation, *Electrochimica Acta* 49 (2003) 85.
- [13] W.P. Zhou, A. Lewera, R. Larsen, R.I. Masel, P.S. Bagus, A. Wieckowski, Size effects in electronic and catalytic properties of unsupported palladium nanoparticles in electrooxidation of formic acid, *Journal of Physical Chemistry B* 110 (2006) 13393.
- [14] H. Miyake, T. Okada, G. Samjeske, M. Osawa, Formic acid electrooxidation on Pd in acidic solutions studied by surface-enhanced infrared absorption spectroscopy, *Physical Chemistry Chemical Physics* 10 (2008) 3662.
- [15] N.W. Maxakato, K.I. Ozoemena, C.J. Arendse, Dynamics of electrocatalytic oxidation of ethylene glycol, methanol and formic acid at MWCNT platform electrochemically modified with Pt/Ru nanoparticles, *Electroanalysis* 22 (2010) 519.
- [16] S. Cherevko, N. Kulyk, C.H. Chung, Nanoporous palladium with sub-10 nm dendrites by electrodeposition for ethanol and ethylene glycol oxidation, *Nanoscale* 4 (2012) 103.
- [17] N. Dalbay, F. Kadrgan, The properties of palladium electrodes for electrooxidation of ethylene-glycol, *Journal of Electroanalytical Chemistry* 296 (1990) 559.
- [18] L. Wang, H. Meng, P.K. Shen, C. Bianchini, F. Vizza, Z. Wei, In situ FTIR spectroelectrochemical study on the mechanism of ethylene glycol electrocatalytic oxidation at a Pd electrode, *Physical Chemistry Chemical Physics* 13 (2011) 2667.
- [19] A. Wolowicz, Use of chelating fibers and ion exchange resins in sorption and separation of Pd(II) ions, *Przemysł Chemiczny* 91 (2012) 53.
- [20] Z.Y. Zhou, X.W. Kang, Y. Song, S.W. Chen, Butylphenyl-functionalized palladium nanoparticles as effective catalysts for the electrooxidation of formic acid, *Chemical Communications* 47 (2011) 6075.
- [21] Z.Y. Zhou, X.W. Kang, Y. Song, S.W. Chen, Enhancement of the electrocatalytic activity of Pt nanoparticles in oxygen reduction by chlorophenyl functionalization, *Chemical Communications* 48 (2012) 3391.
- [22] X.W. Kang, N.B. Zuckerman, J.P. Konopelski, S.W. Chen, Alkyne-functionalized ruthenium nanoparticles: ruthenium-vinylidene bonds at the metal-ligand interface, *Journal of the American Chemical Society* 134 (2012) 1412.
- [23] X.W. Kang, S.W. Chen, Electronic conductivity of alkyne-capped ruthenium nanoparticles, *Nanoscale* 4 (2012) 4183.
- [24] K. Liu, X.W. Kang, Z.Y. Zhou, Y. Song, L.J. Lee, D. Tian, S.W. Chen, Platinum nanoparticles functionalized with acetylene derivatives: electronic conductivity and electrocatalytic activity in oxygen reduction, *Journal of Electroanalytical Chemistry* (2012) <http://dx.doi.org/10.1016/j.jelechem.2012.07.009>
- [25] D.A.J. Rand, R. Woods, Determination of the surface composition of smooth noble metal alloys by cyclic voltammetry, *Journal of Electroanalytical Chemistry* 31 (1971) 29.
- [26] W.J. Zhou, J.Y. Lee, Particle size effects in Pd-catalyzed electrooxidation of formic acid, *Journal of Physical Chemistry C* 112 (2008) 3789.
- [27] C.J. Zhong, J. Luo, B. Fang, B.N. Wanjala, P.N. Njoki, R. Loukrakpam, J. Yin, Nanostructured catalysts in fuel cells, *Nanotechnology* 21 (2010), 062001-1.
- [28] V. Bambagioni, M. Bevilacqua, C. Bianchini, J. Filippi, A. Marchionni, F. Vizza, L.Q. Wang, P.K. Shen, Ethylene glycol electrooxidation on smooth and nanostructured Pd electrodes in alkaline media, *Fuel Cells* 10 (2010) 582.